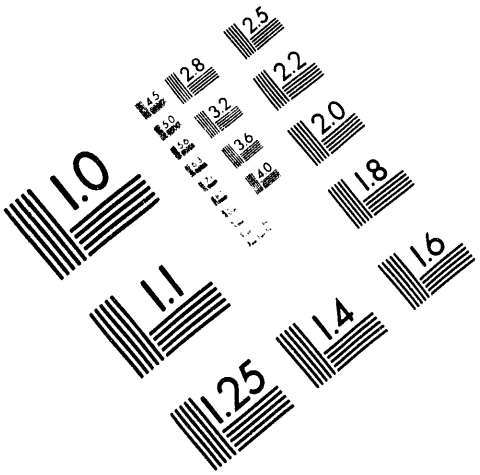

Association for Information and Image Management
1100 Wayne Avenue, Suite 1100
Silver Spring, Maryland 20910
301/587-8202

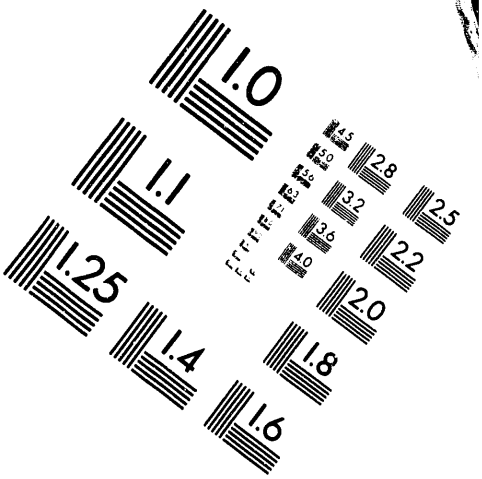

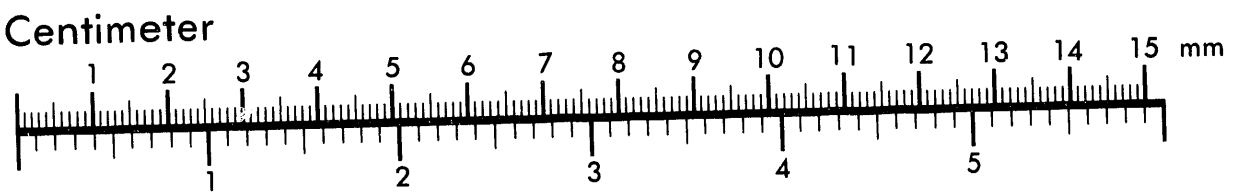

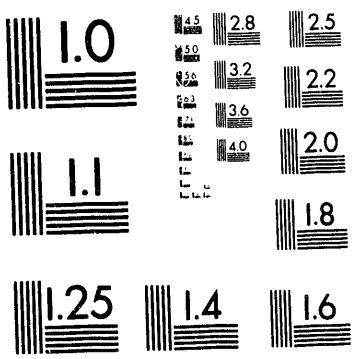

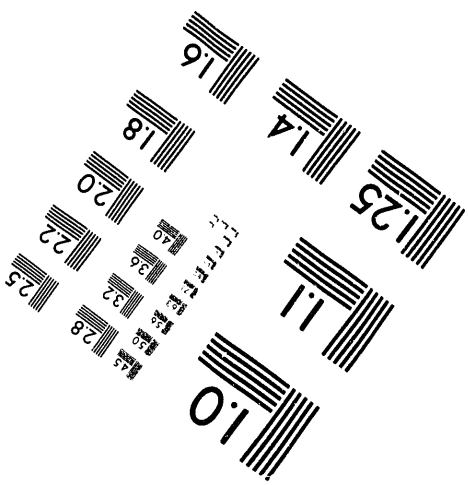

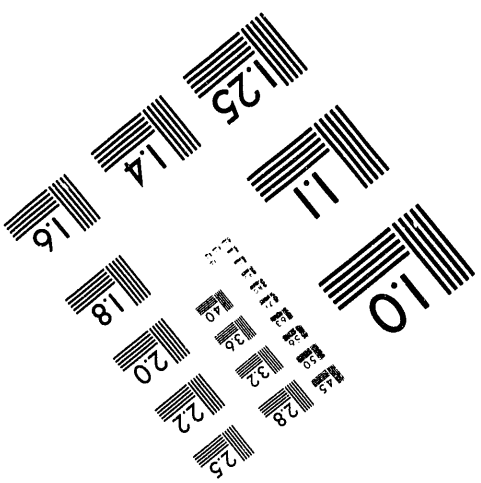

1 of 1

V

CONF-930413/--8

DISCLAIMER

Recent Developments and Applications of the MORSE Code*

S. N. Cramer
Oak Ridge National Laboratory
Radiation Shielding Information Center
P.O. Box 2008
Oak Ridge, TN 37831-6362 USA

ABSTRACT

Several recent analyses using the multigroup MORSE Monte Carlo code are presented. (1) In the calculation of a highly directional-dependent neutron streaming experiment it is shown that P_7 cross section representation produces results virtually identical with those from an analog code. Use has been made here of a recently released ENDF/B-VI data set. (2) In the analysis of neutron distributions inside the water-cooled ORELA accelerator target and positron source, an analytic hydrogen scattering model is incorporated into the otherwise multigroup treatment. (3) The radiation from a nuclear weapon is analyzed in a large concrete building in Nagasaki by coupling MORSE and the DOT discrete ordinates code. The spatial variation of the DOT-generated free-field radiation is utilized, and the building is modeled with the array feature of the MORSE geometry package. (4) An analytic directional biasing, applicable to the discrete scattering angle procedure in MORSE, is combined with the exponential transform. As in more general studies, it is shown that the combined biasing is more efficient than either biasing used separately. Other tracking improvements are included in a difficult streaming and penetration radiation analysis through a concrete structure. Proposals are given for the code generation of the required biasing parameters.

---

*Research sponsored by the U.S. Department of Energy Office of Nuclear Energy, under contract No. DE-AC05-84OR21400 with Martin Marietta Energy Systems, Inc.

The MORSE multigroup Monte Carlo[1,2] code has been in general use worldwide for almost twenty-five years. Although various improvements have been added over the years, the basic framework of the code has remained unchanged. Because of the multigroup cross-section structure no code changes are necessary when new data and formats are released, the necessary changes being made in the cross-section processing codes. The ability to adapt MORSE to almost any type of radiation transport problem, through the use of the user-written routine interface, has enabled many installations to customize the code according to local needs.

One of the potentially serious problem areas in the use of MORSE is low-order P_N expansion for directionally-dependent systems. This is illustrated in the analysis of a neutron streaming experiment shown in Fig. 1.[3] Neutrons are created in the target by the deuteron beam. Small detectors (simulated as points in the analysis) are located at 40 cm off the axis at 3 and 4 meters from the target. A differential analysis has shown that the high-energy neutrons scattered to these detectors are dominated by first collisions near the exit of the duct. In Fig. 2 the flux at the 3 meter detector for a P_3 MORSE calculation is compared to the experimental results and also to an MCNP[4] calculation. The difference in calculational results (both using ENDF/B-V data) virtually disappears when the MORSE cross-section expansion is extended to P_7 (see Fig. 3). Similar results for the 4 meter detector are shown in Figs. 4 and 5. Due to the positions of the two detectors relative to the first collision sites, the P_3 results are too high in one case and too low in the other. The analysis of this experimental system was initially involved with attempting to resolve the experimental-calculational discrepancies in the high-energy peak, and not as a companion of calculational methods and codes. The discrepancies remain unresolved, but the results illustrate the proper utilization of the P_N expansion. MORSE calculations have also been made for the two detectors using ENDF/B-VI data (collapsed from the VITAMIN-J group structure for comparison with the VITAMIN-E structure),[5] but no improvement in the high-energy comparisons from Fig. 3 and 5 were found. There was some change in the low, intermediate-energy fluxes, where the uncertainty in all results is the greatest and where the difference in the two Monte Carlo code scattering models and data can be seen.

The use of a few energy groups to cover wide energy ranges has also been a source of error for any multigroup cross-section method of analysis. However, with large sets such as the 174-38 group neutron-photon VITAMIN-E library now in general use, this source of error has greatly diminished. This library has been used in MORSE, with a P_5 expansion, in the neutron analysis of the Oak Ridge Electron Linear Accelerator (ORELA) target and positron source system,[6] both water-cooled and shown schematically in Figs. 6 and 7. The energy range covered was 20 MeV to 10 eV. The electron beam produces a bremsstrahlung photon source in the tantalum plates, which then produces neutrons via photoneutron reactions and positrons via pair production in aluminum-clad tungsten plates. The neutrons are collected into beam tubes of various lengths for time-of-flight cross-section measurements. Of particular interest was the calculation of the delay time distributions (resolution function) of the neutrons inside the target between birth (electron pulse)

and escape into the flight tube. This resolution function was computed in MORSE by redefining the time variable as a distance equal to the elapsed time in the target multiplied by the neutron mid-group velocity at escape. A second change introduced into the code was an analytic hydrogen scattering model to more properly account for neutron collisions with hydrogen in the cooling water of both the target and positron source. An extra cross-section mixture for hydrogen, with an atomic density of that for the nuclide in water, was made available in the standard mixing procedure. For each collision in water a random determination was made of the struck nuclide using this extra data. An oxygen collision proceeded in the normal multigroup mode, but for hydrogen the outgoing direction and energy were determined analytically and then re-coupled with the standard method. A third non-standard feature of the ORELA target analysis consisted of a next-event type coupling calculation from the target to the positron source, then following neutron collisions there, a second coupling back into the target. In this manner the effect of neutron backscatter from the positron source on the target resolution function could be determined. The positron extraction tube, located further from the target, was ignored. A typical set of calculated data is shown in Fig. 8 in the form of the probability of an effective neutron distance in the target at escape. The two components of this data were not analyzed experimentally. The calculated leakage spectra from the target is shown in Fig. 9 and compared with an earlier, less detailed model analysis using a continuous-energy code.[7] Here a shadow bar, blocking the neutron escape from the tantalum plate area, was simulated in both calculations. In Fig. 10 the MORSE-calculated effective distance spectrum is shown. The slight maximum and then high-energy decline of the distributions, for escape from the tantalum plate area only, has been observed experimentally.

In another analysis using MORSE, several code features and applications of multigroup Monte Carlo are presented: (1) general discrete ordinate-Monte Carlo coupling, (2) adjoint mode of operation, (3) forward flux spectra from adjoint calculations, and (4) array geometry capability. The calculations are for radiation doses and neutron activation at various locations in Hiroshima and Nagasaki due to the nuclear weapon detonations over these cities in World War II.[8] The coupling geometry is shown in Fig. 11, and the source point is on the central cylindrical axis (not shown). The forward discrete ordinate free-field, air-over-ground angular flux is made available at the indicated node points in the cylindrical volume element by a calculational sweep through the angle $\Delta\psi$. When an adjoint Monte Carlo particle escapes the interior geometry, the appropriate discrete ordinate forward flux is determined by interpolations in space, closest polar angle cosine and azimuthal angle, and one-to-one correspondence in energy group. The result is given for general phase space coordinate ρ

$$\lambda = \int_{\vec{n}\cdot\vec{\Omega}>0} \phi(\rho)\phi^*(\rho)(\vec{n}\cdot\vec{\Omega})d\rho \qquad (1)$$

where $\phi(\rho)$ is $\phi_{g'}$, the discrete ordinate flux in group g', and $\phi^*(\rho)(\bar{n}\cdot\bar{\Omega})$ is the adjoint leakage current $J^*_{gg''}$. This coupling procedure represents an increased capability over the much-used DOMINO code,[9] in which the MORSE geometry must be exterior to the entire cylinder of the discrete ordinates calculation ($\Delta\psi$ must be 2π). The forward flux in group g at the adjoint source point (detector location) is determined by

$$\phi_g = 4\pi N \sum_{g'} \int_{\substack{\text{coupling}\\ \text{surface}}} \int_{\bar{n}\cdot\Omega>0} J^*_{gg''}\ \phi_{g'}\ d\bar{\Omega}d\bar{r} \qquad (2)$$

where the adjoint group number at escape is $g''=N-g'+1$, N is the total number of groups, and $4\pi N$ is the adjoint source normalization.[2] The adjoint source group g is selected uniformly within the N groups and this value is retained by the particle history and used to score in the above integral at escape. In the evaluation of an energy-integrated quantity the adjoint source g is selected from an energy-dependent response function, and no further reference is made to this group number. In the application of this coupling procedure, a large concrete building in Nagasaki was modeled as shown in Fig. 12. It was placed inside the coupling system replacing the geometry in Fig. 11 at the proper orientation as indicated in Fig. 12, approximately 500 meters ground range from and 500 meters below the detonation point. The vertical and horizontal lines on the exterior of the building represent the array matrix, into which individually modeled segments of the building were placed by appropriate input instructions. The results of the calculation were given as radiation reduction factors at locations interior to the building relative to the free field radiation at those locations with no building present. For the weapon neutron output only, the reduction factors at the center of the building on the first floor were calculated by the coupling method to be $14\pm8\%$ for neutron dose and $27\pm12\%$ for secondary photon dose. The three-dimensional code TORT[10] computed these values to be 13 and 26, respectively.

All the above analyses were made with an ORNL in-house version of MORSE which uses combined directional and path length biasing.[11] The advantages of this combined biasing scheme are (1) the outgoing direction after collision is preferentially biased toward (or away from) the same point toward which path lengths are preferentially stretched (or shortened), (2) undesirable weigh correction fluctuations that occur when either biasing is used separately are reduced, (3) the method is problem independent, (4) the general method is a direct consequence of manipulations with the Boltzmann transport equation, (5) the importance region geometry of a complicated calculational system can be simplified from that with other forms of biasing, although the user-written DIREC routine defining the preferential direction for each importance region is still required, (6) only one empirical parameter is required for both biasings, and (7) for a code with discrete scattering angles such as MORSE, the biasing application is analytic in contrast to a numerical integration at each collision required for general application.

In MORSE the biased collision kernel is

$$\tilde{C} = \frac{C}{N(1-p\mu)} \tag{3}$$

where

C = the unbiased kernel

p = the empirical biasing parameter, $0<p<1$

μ = the cosine of the angle between the preferential direction $\bar{\Omega}_0$ and the outgoing direction $\bar{\Omega}$ to be selected (see Fig. 13; $\bar{\Omega}'$ is the incident direction)

N = normalization constant

The biased transport kernel for the selection of the mean free path η is

$$\tilde{T} = (1-p\mu)e^{-(1-p\mu)\eta} , \tag{4}$$

and the combined weight correction is (applied separately in different parts of the code)

$$WT = (C/\tilde{C})\ (T/\tilde{T}) = Ne^{-p\mu\eta} . \tag{5}$$

The biased distribution for the discrete scattering angle selection is

$$f_n' = \frac{\int_{-\pi}^{\pi} \frac{f_n d\phi}{(1-p\mu)}}{\sum_{i=1}^{L} \int_{-\pi}^{\pi} \frac{f_i d\phi}{(1-p\mu)}} , \tag{6}$$

where f_i is the unbiased probability for scattering angle cosine μ_i and L is the expansion order. From Fig. 13

$$\mu = \mu_i\mu_0 + \sqrt{1-\mu_i^2}\,\sqrt{1-\mu_0^2}\,\cos\phi \ , \tag{7}$$

the distribution for the azimuthal angle is,

$$P_n' = \frac{\dfrac{1}{1-p\mu_n}}{\displaystyle\int_{-\pi}^{\pi} \frac{dp}{(1-p\mu_n)}} \ , \tag{8}$$

and

$$\tan\frac{\phi}{2} = \sqrt{\frac{1-p\mu_{nx}}{1-p\mu_{nm}}}\,\tan\left[\pi\left[RN-\frac{1}{2}\right]\right] \ , \tag{9}$$

where μ_{nx} and μ_{nm} are the values of μ_n for ϕ=0 and π, respectively in Eq. (7), and RN is a uniform random number on the unit interval. The ϕ from Eq. (9) must be given a final adjustment, $\psi = \phi+\phi'$, where using the cosine components of $\bar{\Omega}'$ and $\bar{\Omega}_0$

$$\cos\phi' = \frac{\mu_0 W' - W_0}{\sqrt{1-\mu_0^2}\sqrt{1-W'^2}} \ , \tag{10}$$

and

$$\sin\phi' = \frac{U'V_0 - U_0V'}{\sqrt{1-\mu_0^2}\sqrt{1-W'^2}} \ . \tag{11}$$

The normalization constant in Eq. (5) is

$$N = \sum_{i=1}^{L} \frac{f_i}{\sqrt{1-p\mu_{ix}}\sqrt{1-p\mu_{im}}} \ . \tag{12}$$

In order to capitalize on the combined biasing scheme, two other changes should be made in MORSE: (1) the transport process should be interrupted at importance region

boundaries so that changes in $\bar{\Omega}_0$ and p can be made [even without collision and path length biasing this should be done in order to permit boundary splitting and Russian roulette; i.e., call TESTW from BANKR(7)[12]], and (2) apply collision splitting and Russian roulette after both the collision and transport processes are completed, not between them. The programming changes necessary to implement the combined biasing into MORSE are given in Appendix F of Ref. 13 with corrections for P_N, $N>3$, in Ref. 14 (page 11).

The original analysis using the combined biasing in MORSE consisted of an experimental system simulating a concrete building shown in Fig. 14. The entire system is shown sch matically in Fig. 15. Neutrons and photons from the Oak Ridge Tower Shielding Reactor and spectrum modifier impinge on the front face of the structure. The source for the MORSE calculation at the exit of the spectrum modifier was adjusted to agree in magnitude with experimental values. TLD energy deposition is computed at the indicated detector locations and compared with experimental results, as *C/E* ratios, in Table. I.

In the combined biasing study, proposals are given for the possible code generation of the $\bar{\Omega}_0$ and p as adjoint flux-weighted values for an importance volume V_l of the form, for a general parameter ω_l[11]

$$\omega_l = \frac{\int_{V_l} \omega(\rho)\phi^*(\rho)d\rho}{\int_{V_l} \phi^*(\rho)d\rho}, \tag{13}$$

where the value of ω for each history created in or passing through V_l is carried with it until a contribution to the desired result by that history is made at the detector. The adjoint flux is accumulated in the forward calculation in the same general manner as for the forward flux in the adjoint application for Eq. (2). This parameter generation method has not been completely successful in reduced variance and increased efficiency in general applications and is still under development. However, it is recommended that the combined biasing scheme, with empirical parameters p, be included in any MORSE code system, as well as boundary splitting and Russian roulette and the analytic hydrogen scattering model. Several features of the next-event estimation routines should also be considered: (1) for photon calculations use of the Klein-Nashina equation for Compton scattering[15] significantly reduces the statistical uncertainty from the standard routine (this routine also accounts for pair production and the photoelectric effect), (2) estimation to all energy groups,[2] (3) ring detectors for azimuthally symmetric detectors,[16] and (4) estimation to finite detectors.[2,6,15,17,18]

Table I. Detector response comparisons inside the concrete building.

Detector in Fig. 15	Experimental Response[a]	C/E	Calculated uncertainty[b] (%)	Fractional response and uncertainty from source segmentation					
				Uncollided		Front face		Other	
					(%)		(%)		(%)
1	1.33	0.96	2.7	0.128	0.4	0.702	2.6	0.170	11.7
2	6.73	0.99	0.4	0.802	0.3	0.122	2.3	0.076	2.0
3	1.36	1.00	3.6	0.129	0.4	0.732	2.9	0.139	20.9
4	5.41	0.99	0.4	0.816	0.3	0.128	1.4	0.056	4.7
5	1.11	0.92	4.4	0.136	0.4	0.629	1.9	0.235	18.0
6	3.84	1.01	0.4	0.837	0.3	0.120	1.6	0.043	5.7
7	0.24	0.98	9.1	0.001	0.8	0.756	6.0	0.243	32.5
8	1.23	1.12	1.6	0.578	0.6	0.354	4.0	0.068	9.7
9	2.80	1.07	0.7	0.762	0.3	0.206	3.1	0.032	5.4
10	0.28	1.14	6.0	0.001	0.8	0.722	3.6	0.267	20.3

[a]TLD energy deposition in MeV · g^{-1} · min^{-1} · kW^{-1} × 10^{-4} from *Nucl. Sci. Eng.*, 98, 279–98 (1988), with experimental uncertainty ~5%.
[b]One standard deviation as a percent of the calculated response.

REFERENCES

1. M. B. Emmett, *MORSE-CGA, A Monte Carlo Radiation Transport Code with Array Geometry Capability*, ORNL-6174 (1985).

2. S. N. Cramer, *Applications Guide to the MORSE Monte Carlo Code*, ORNL/TM-9355 (1985).

3. S. N. Cramer and T. Y. Lee, "Monte Carlo Analysis of a Neutron Streaming Experiment," *Nucl. Sci. Eng.*, 107, 180–87 (1991).

4. J. F. Briesmeister, Ed., *MCNP — A General Monte Carlo Code for Neutron and Photon Transport, Version 3A*, LA-7396-M, Rev. 2, Los Alamos National Laboratory (1986).

5. J. E. White, private communications, Oak Ridge National Laboratory (1992).

6. S. N. Cramer and F. G. Perey, "Time-Dependent Monte Carlo Calculations of the Oak Ridge Electron Linear Accelerator Target Neutron Spectrum," *Nucl. Sci. Eng.*, 111, 102–11 (1992).

7. C. Coceva *et al*, "Calculation of the ORELA Neutron Moderator Spectrum and Resolution Function," *Nucl. Instrum. Meth.*, 211, 459 (1983).

8. S. N. Cramer and C. O. Slater, *Investigation of Radiation Effects in Hiroshima and Nagasaki Using a General Monte Carlo-Discrete Ordinates Coupling Scheme*, ORNL/TM-11532 (1990).

9. M. B. Emmett, *DOMINO-II, A General Purpose Code for Coupling DOT-IV Discrete Ordinates and Monte Carlo Radiation Transport Calculations*, ORNL/TM-7771 (1981).

10. W. A. Rhoades *et al*, *Radiation Exposure Inside Reinforced Concrete Buildings at Nagasaki*, ORNL/TM-10589 (1989).

11. S. N. Cramer, "Angle Biasing in Monte Carlo Radiation Transport," *Nucl. Sci. Eng.*, 98, 279–98 (1988).

12. S. N. Cramer, unpublished notes, RSIC Workshop on the MORSE Code (1985).

13. S. N. Cramer, *Discrete Angle Biasing in Monte Carlo Radiation Transport*, ORNL/RSIC-50 (1988).

14. T. Y. Lee and S. N. Cramer, *Neutron Streaming Benchmark Calculations*, ORNL/RSIC-52 (1989).

15. S. N. Cramer, "Adjoint Gamma-Ray Estimation to the Surface of a Cylinder — Analysis of a Remote Reprocessing Facility," *Nucl. Sci. Eng.*, 79, 417–25 (1981).

16. T. J. Hoffman and J. S. Tang, *XSDRNPM-S Biasing of MORSE-SGC/S Shipping Cask Calculations*, ORNL/SSD/TM-175;NUREG/CR-2342 (1982).

17. S. N. Cramer and J. S. Tang, *Variance Reduction Methods Applied to Deep-Penetration Monte Carlo Problems*, ORNL/TM-9643 (1986).

18. S. N. Cramer, "Analytic Estimation of Radiation Effects in Space Using Solid Angles," in *Nuclear Technologies for Space Exploration*, ANS NTSE-92, Vol. III, Jackson, Wyoming (1992).

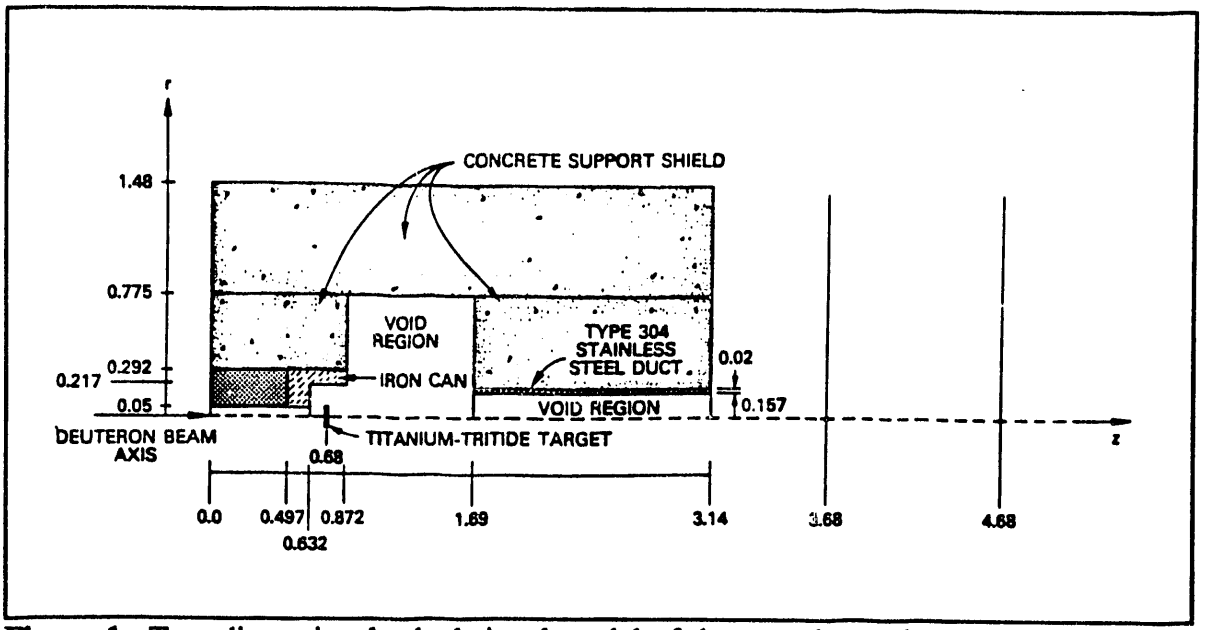

Figure 1 Two-dimensional calculational model of the experimental geometry. All dimensions are in meters.

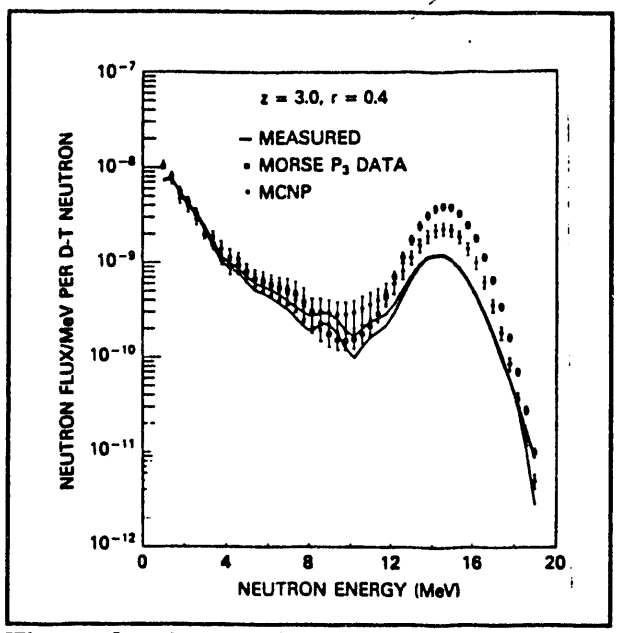

Figure 2 Neutron flux per unit energy versus neutron energy for the detector at z = 3 m and r = 0.4 m. The order of scattering of the MORSE calculation is P_3.

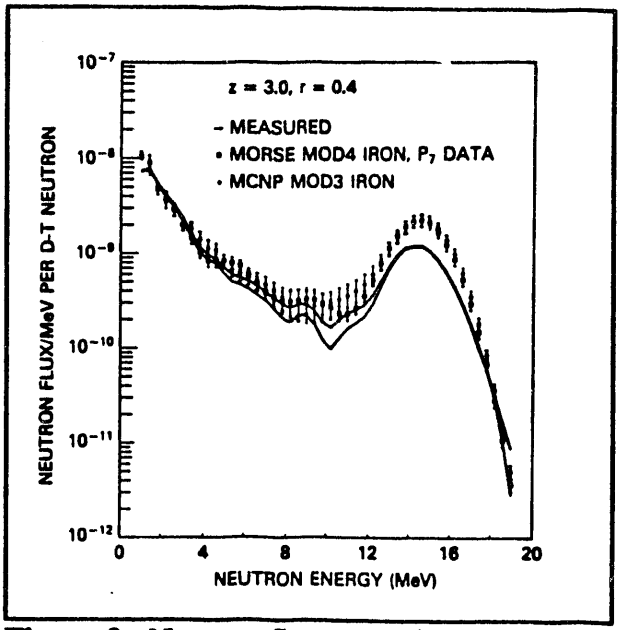

Figure 3 Neutron flux per unit energy versus neutron energy for the detector at z = 3 m and r = 0.4 m. The order of scattering of the MORSE calculation is P_7.

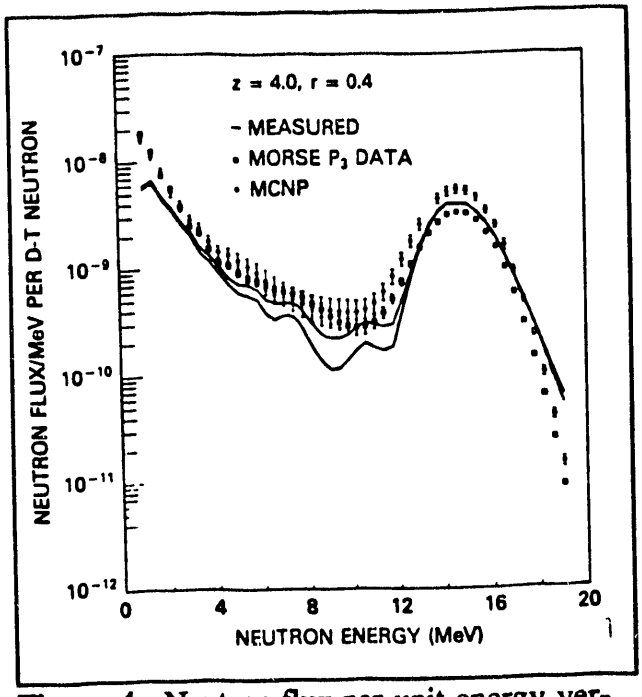

Figure 4 Neutron flux per unit energy versus neutron energy for the detector at $z = 4$ m and $r = 0.4$ m. The order of scattering of the MORSE calculation is P_3.

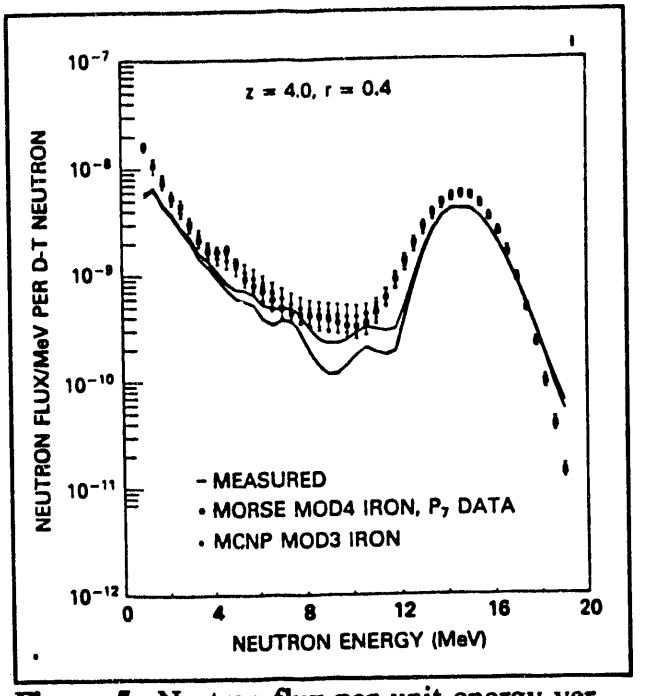

Figure 5 Neutron flux per unit energy versus neutron energy for the detector at $z = 4$ m and $r = 0.4$ m. The order of scattering of the MORSE calculation is P_7.

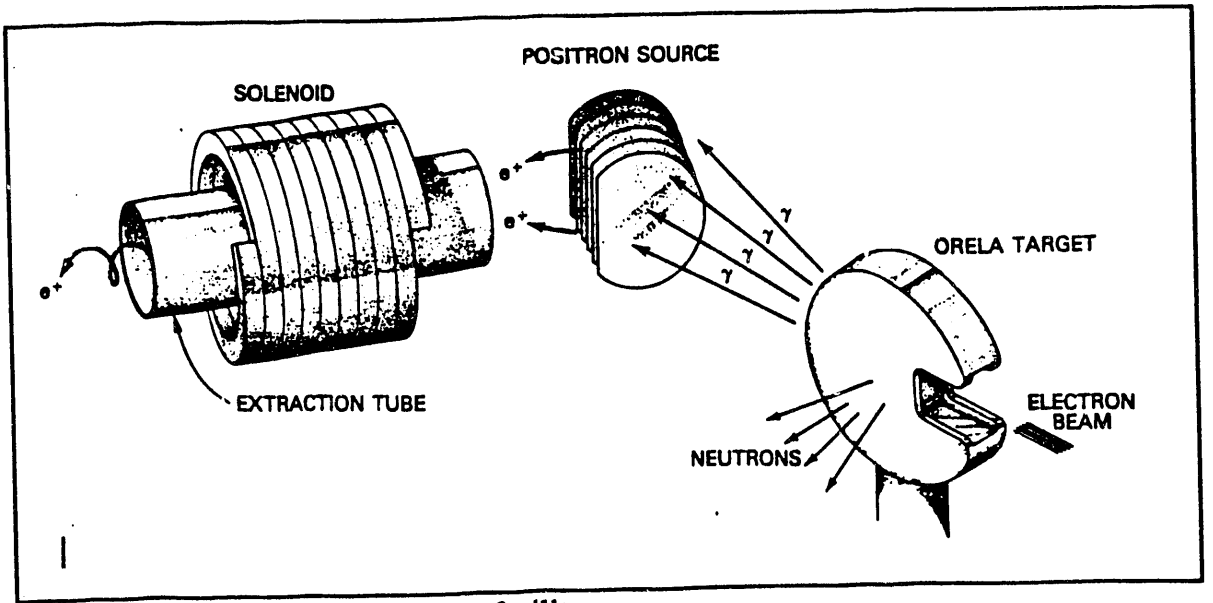

Figure 6 ORELA positron source facility.

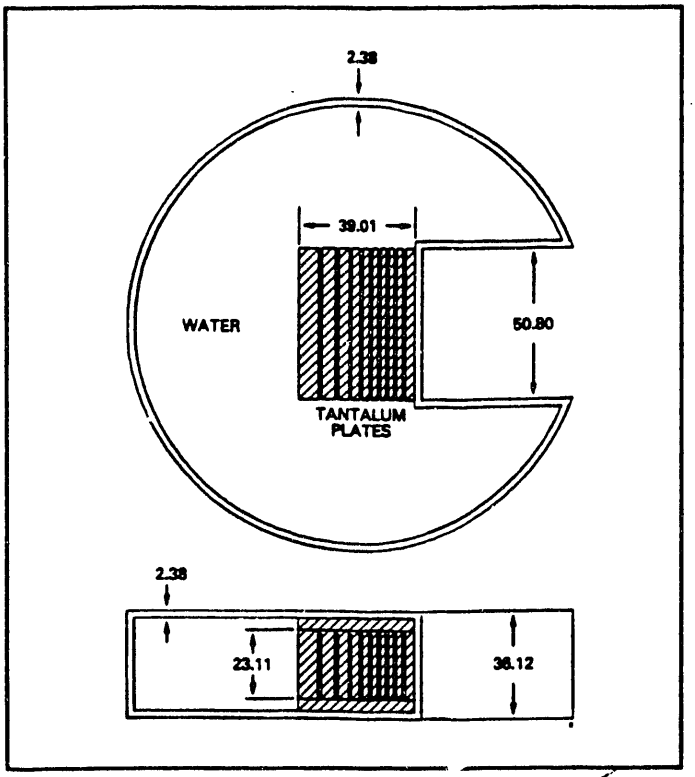

Figure 7. Model of the 15.24-cm-diam ORELA target (dimensions are given in millimeters).

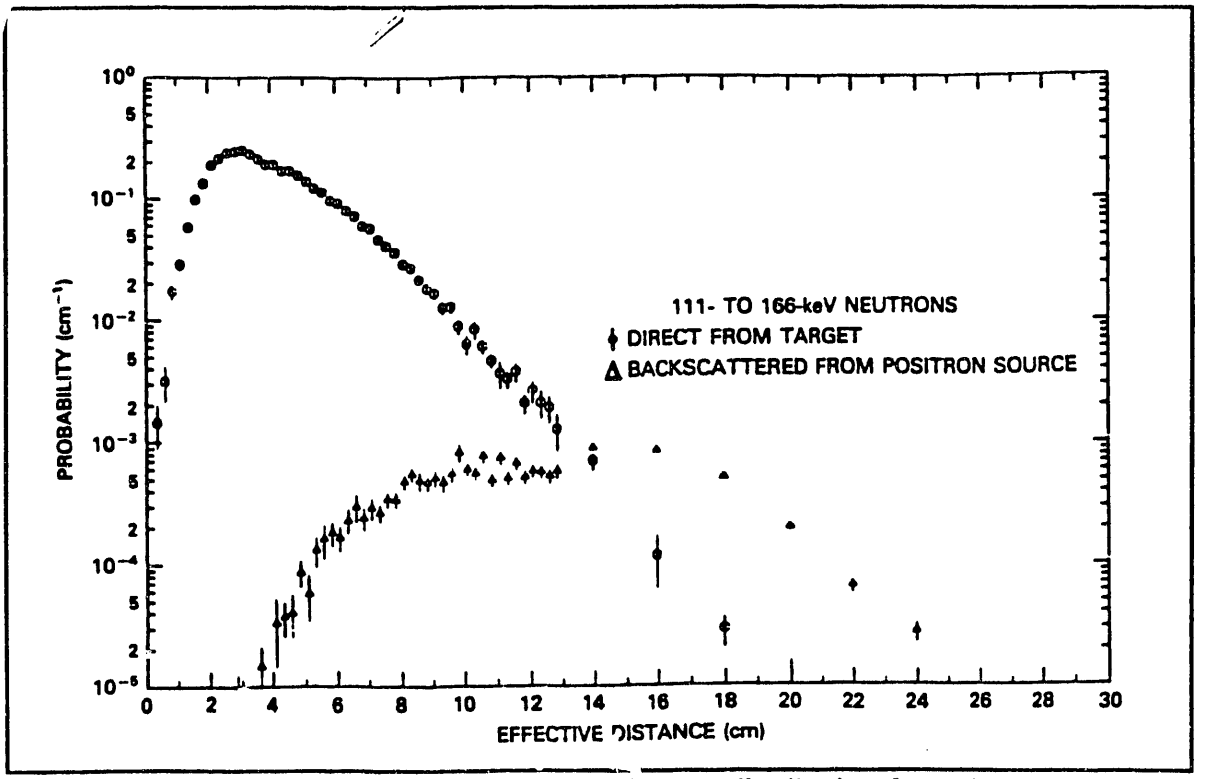

Figure 8 Direct and backscattered effective distance distribution from the ORELA target.

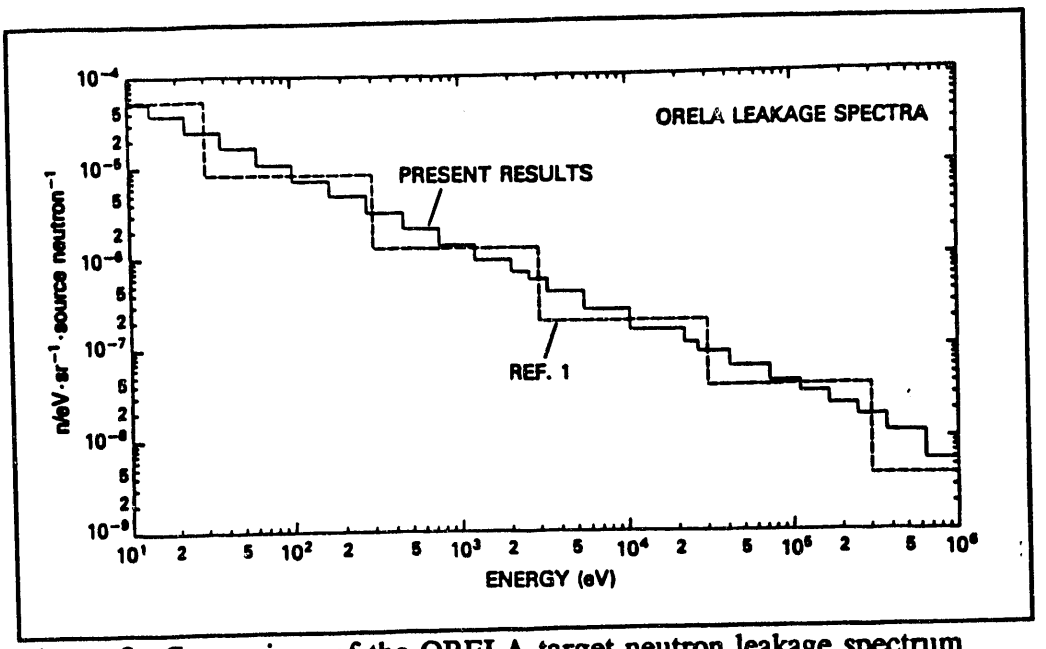

Figure 9 Comparison of the ORELA target neutron leakage spectrum with the tantalum plates blocked out.

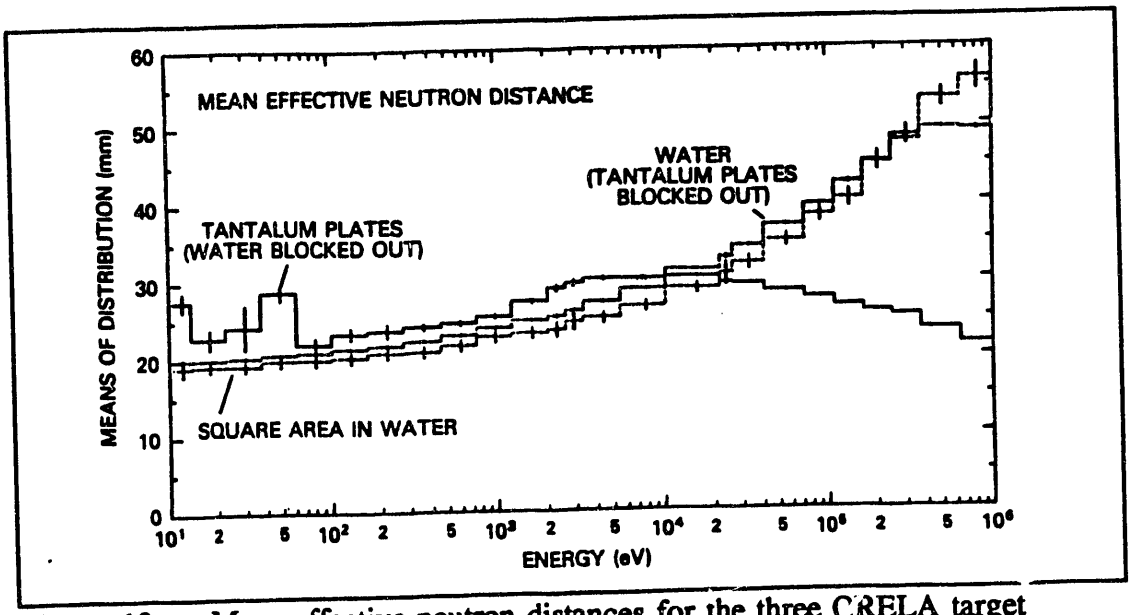

Figure 10 Mean effective neutron distances for the three ORELA target leakage configurations.

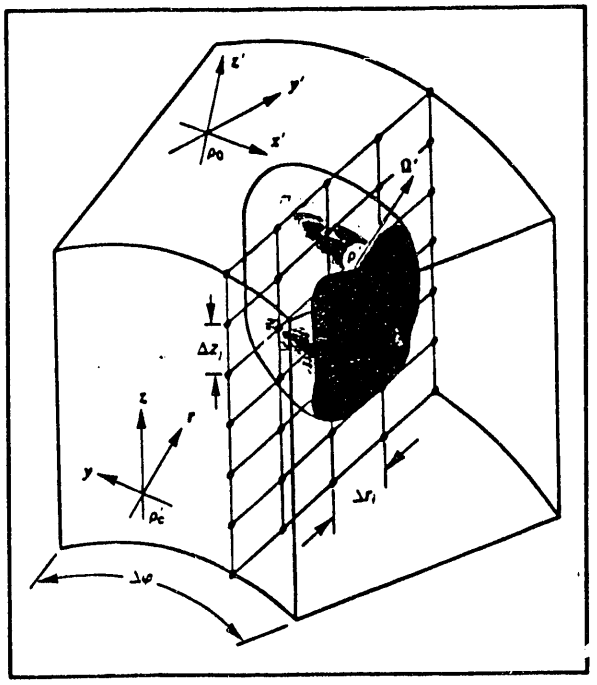

Figure 11. Monte Carlo geometry and discrete ordinates flux grid.

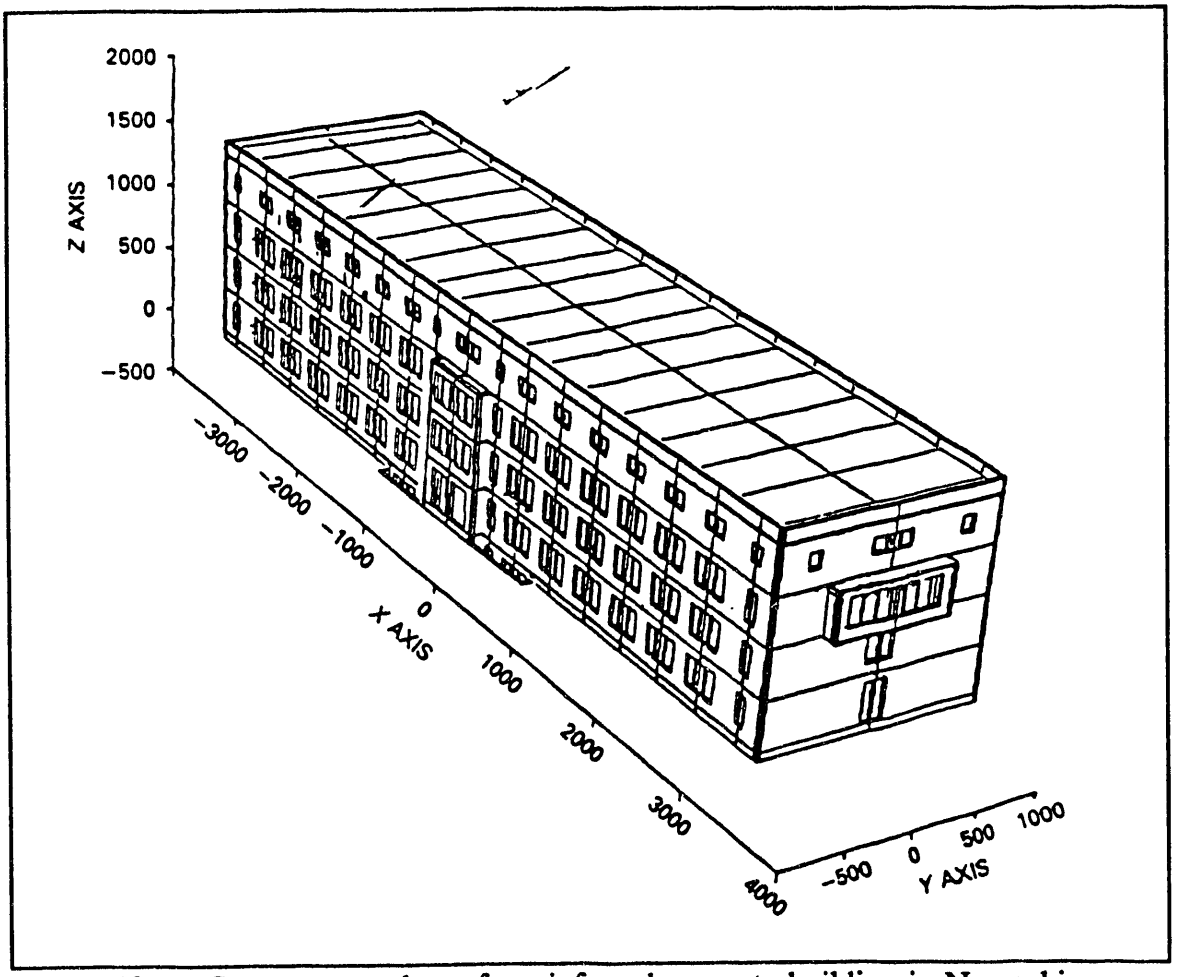

Figure 12 Computer mockup of a reinforced concrete building in Nagasaki.

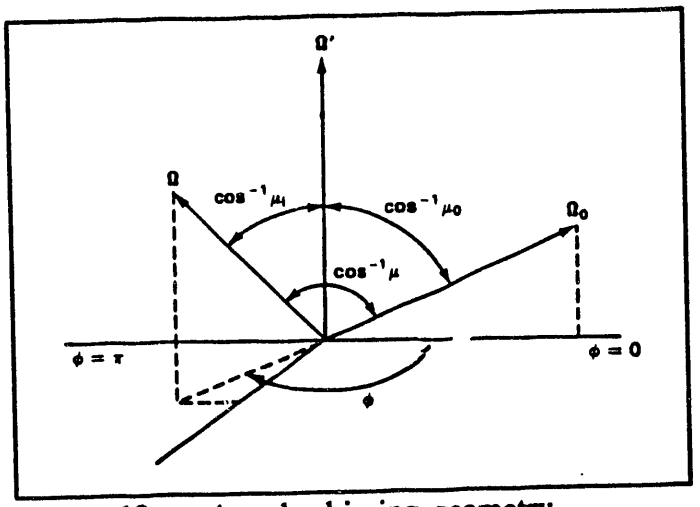

Figure 13 Angular biasing geometry.

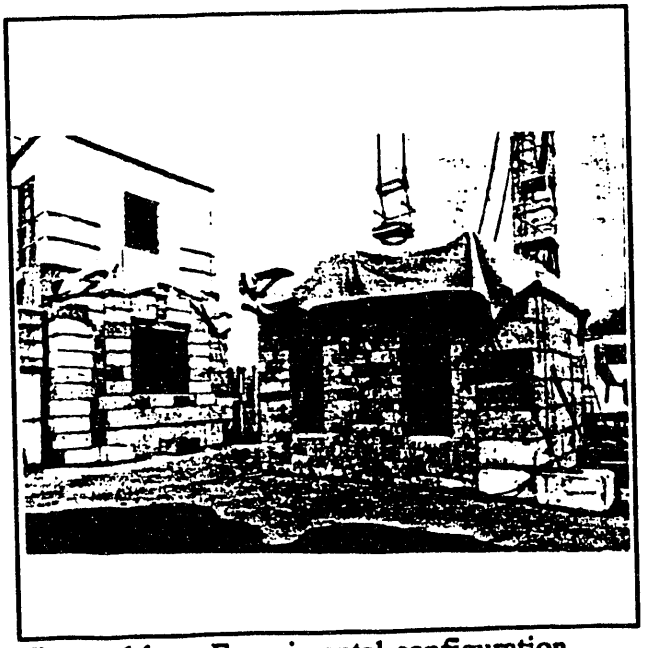

Figure 14 Experimental configuration showing the spectrum modifier on the left and the concrete block house on the right.

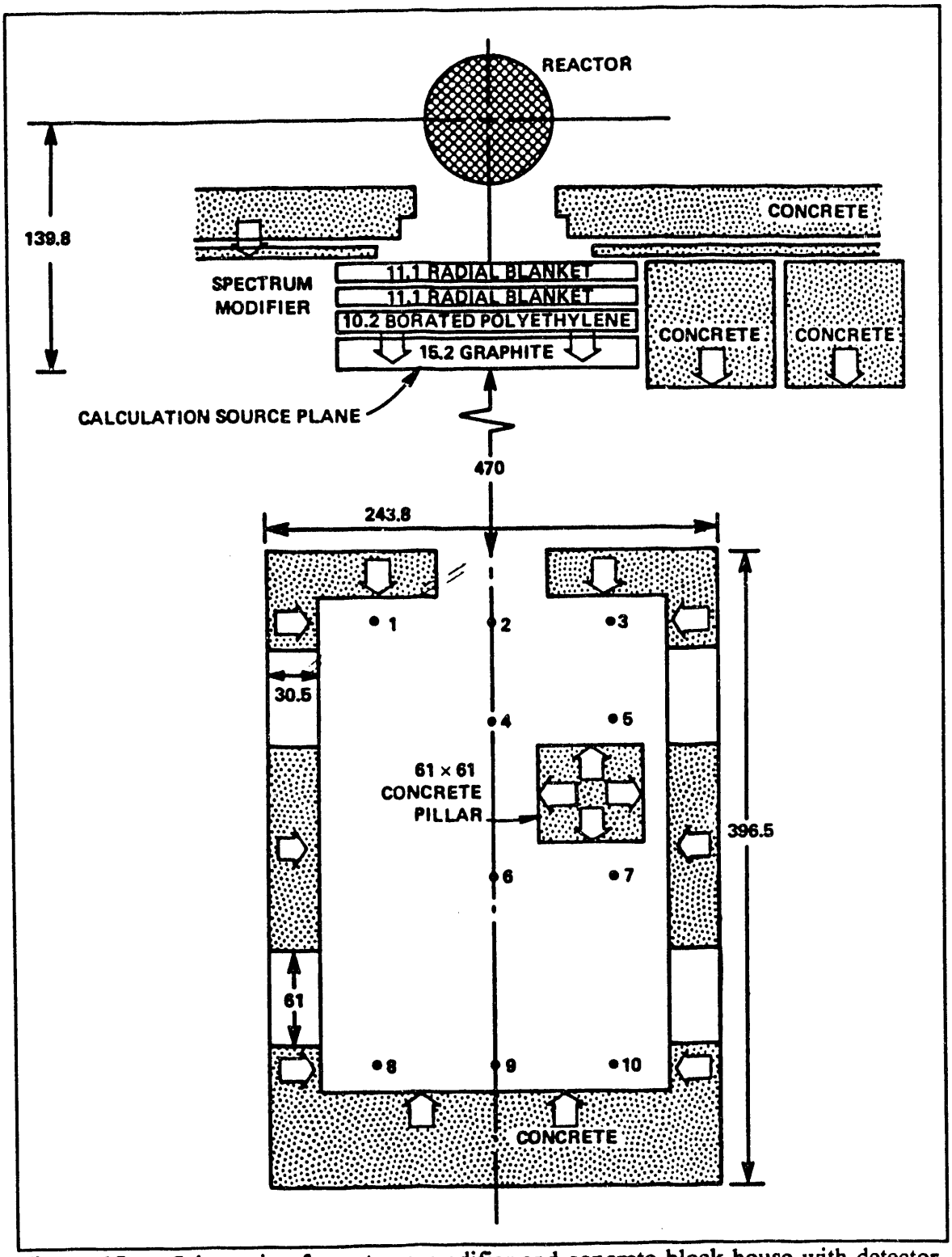

Figure 15 Schematic of spectrum modifier and concrete block house with detector locations and preferential directions ω_0 (large arrows) used in calculations. All dimensions are in centimeters.

DATE
FILMED
9/10/93

END